https://doi.org/10.5194/egusphere-2025-3637
Preprint. Discussion started: 21 August 2025

Measurement Report: New insights into the boundary layer revolution impact on new particle formation characteristics in three megacities of China

Hancheng Hu[1], Yidan Zhang [1], Yuting Li[1], Dongyang Pu [1], Hao Wu[1,*]

1College of Electronic Engineering, Chengdu University of Information Technology, Chengdu 610225

* Correspondence: wuhao@cuit.edu.cn; 86 18613878407

Abstract: New particle formation (NPF) events contribute more than 60% of ultrafine particles particularly in the boundary layer. This study retrieved the particle number size distribution and the NPF parameters and their relationship with planetary boundary layer height (PBLH) evolution, as well as the air mass back trajectories during NPF events in three Chinese cities: Beijing, Guangzhou, and Shanghai. Furthermore, all NPF events has been classified into three types: new particles grow rapidly during the initial rise of the boundary layer in Type I events, while they grow after the boundary layer reaches a certain height (above 800 m) in Type II events, and the shrinkage cases are the Type III. The results show that particle growth dynamics categorized into distinct types demonstrate that sustained particle growth predominantly occurred under conditions of stable and elevated PBLH. Survival parameters ranged from 13.1 to 115.9 in Beijing, 9.0 to 110.2 in Guangzhou, and 8.4 to 25.6 in Shanghai. Specifically, Type I events were associated with survival parameters between 14.0 and 45.2. A significant negative correlation is observed between survival parameters and PBLH ($R^2 = 0.2$ in Beijing, $R^2 = 0.02$ in Guangzhou, and $R^2 = 0.99$ in Shanghai, respectively). The main source of Aitken mode transport to Beijing is from Mongolia region. In Guangzhou, the contribution mainly comes from Jiangxi and Fujian provinces located in the northeast, while in Shanghai, the source lies to the northwest. This research provides valuable insights into developing strategies to manage the atmospheric environment.

Keywords: new particle formation; planetary boundary layer height; parameter correlation; backward trajectory.

1. Introduction

https://doi.org/10.5194/egusphere-2025-3637
Preprint. Discussion started: 21 August 2025

New particle formation (NPF) is the process by which detectable nanoscale clusters are formed through heterogeneous nucleation of supersaturated gas molecules in the atmosphere (Kanawade et al., 2022). This phenomenon occurs with remarkable regularity in the atmosphere and culminates in the formation of significant nucleation mode aerosol particles through condensation and coagulation. These newly formed particles evolve over spatial scales of hundreds of kilometers and timescales of 1–2 days, potentially affecting the global climate as cloud condensation nuclei (CCN) (Zhao et al., 2017; Kerminen et al., 2018). NPF events occur frequently in various atmospheric environments (Li et al., 2023b), playing a major role in the evolution of particle number concentration. The processes of early nucleation, continuous growth and occurrence frequency are critical issues in aerosol formation and Ultrafine particle source research. Exploring its relevant mechanisms has significant impacts on regional environmental quality, climate, and human health (Kulmala et al., 2022). Currently, many methods have been used to identify the growth characteristics and development mechanisms of NPF (Hu et al., 2016; Chan et al., 2020), such as field observations (Kerminen et al., 2018), model simulations and smoke chamber simulations (Chu et al., 2022). Among these, model simulations and smoke chamber simulations are usually employed to study the chemical mechanisms of NPF.Especially in the boundary layer, most NPF are under the control of the daily evolution of the planetary boundary layer height (PBLH) (Du et al., 2025; Sun et al., 2015)so the influence should be further studied.

In China, research on NPF process parameters has been conducted through field observations in multiple locations, including Beijing (Kulmala et al., 2021; Wu et al., 2021b) and the Northwest Desert region (Shengjie et al., 2001). A long-term (373 days) observation of NPF in urban Beijing examined the formation and growth of sub-3 nm particles. It found that a sluggish growth rate (GR) and the presence of pristine background aerosols lead to a reduced survival rate of newly formed particles (Deng et al., 2021a). Moreover, ultrafine particles (UFP, diameter < 100nm) are greatly affected by the condensation sink (CS), with 95% of NPF events occurring when CS $<$ 0.03 s^{-}

https://doi.org/10.5194/egusphere-2025-3637
Preprint. Discussion started: 21 August 2025

[1] (Deng et al., 2021b). The impact of PBLH on NPF is complex and significant, involving multiple factors such as meteorological conditions, precursor gas concentrations, and particle growth mechanisms. Various atmospheric conditions influence not only the frequency of NPF but also its development. High relative humility could be responsible for the enhanced growth (Du et al., 2025) and at the higher temperature the cluster evaporation markedly slows NPF (Li et al., 2023a). Furthermore, due to the lower availability of condensable species, NPF events occurring under cleaner atmospheric conditions exhibit lower GR of newly formed particles (Bousiotis et al., 2018). The relationship between PBLH and NPF is intricate and warrants further in-depth research.

As a key process of air pollution, NPF can change boundary layer structure directly or indirectly by influencing the surface energy balance through radiation effects (Myhre et al., 2013). Shen et al. (2016) reported the diurnal variation in NPF number concentration observed at Mount Tai is primarily governed by the evolution of the boundary layer, while the seasonal variation is driven by both boundary layer evolution and atmospheric advection over Mount Tai. Deot et al. (2024) conducted measurements at different altitudes in Cyprus and found that higher PBLH are typically associated with stronger NPF events, which attributed to under higher boundary layer conditions, more precursor gases can accumulate at elevated temperatures and with lower CS rates. The boundary layer development can govern the capacity for atmospheric vertical diffusion, and changes in its height will directly affect the transport process of NPF, indicating a direct feedback system between NPF and the PBL. The influence of NPF on the PBLH varies with seasonal conditions: during colder periods (autumn and winter), lower PBLH correlates negatively with nucleation-mode particle (Nuc mode), while in warmer periods (spring and summer), lower PBLH correlates positively with NPF events (Blanco-Alegre et al., 2022). In warmer periods (spring and summer), higher PBLH supports NPF by enhancing vertical mixing and creating a cleaner atmosphere (Blanco-Alegre et al., 2022). Additionally, high aerosol concentrations in

https://doi.org/10.5194/egusphere-2025-3637
Preprint. Discussion started: 21 August 2025

the PBL can suppress NPF by reducing particle sources and increasing sinks, shifting NPF occurrences to the lower troposphere (Quan and Jia, 2020). The flux of harmful aerosol pollution in the boundary layer depends on atmospheric turbulent mixing, which is closely related to the PBLH (Stjern et al., 2023). A high CS environment can hinder the growth of new particles, while the boundary layer can affect CS, thereby influencing NPF. The PBLH impacts the vertical distribution of particles (Wu et al., 2021a). The PBLH influences the distribution and concentration of particles (Wang et al., 2021), which in turn affects the CS by altering the surface area available for vapor condensation (Sebastian et al., 2021).

However, long-term observations of NPF are rare in China, with only a few studies documenting NPF observations spanning more than one year (Peng et al., 2017; Chu et al., 2019). In this study, we utilized long-term observational datasets to analyze particle variations, backward trajectories, and pollution distribution maps of megacities (Beijing, BJ; Guangzhou, GZ; Shanghai, SH) in China during NPF periods. We use the same setup and observation procedure around the cities. The effective observation days of BJ, GZ, and SH were 408, 127, and 53 days, respectively. The back trajectory is estimated from the Hybrid Single-Particle Lagrangian Integrated Trajectory (HYSPLIT) model developed by the NOAA Air Resources Laboratory. This approach considers the diversity of different natural atmospheric conditions and human activities, providing a basis for clarifying the similarities and differences in the sources and transport processes of particulate pollutants across different megacities regions in China mainland.

The research methods and locations of the observation sites are presented in Chapter 2. Chapter 3 discusses the occurrence frequency of NPF, the seasonal daily variations in aerosol PNSD at the three sites, and the 48-hour backward trajectories of particulate matter during NPF events. Additionally, we conducted research on the PBLH of the three cities during NPF events. This study provides an important reference for

https://doi.org/10.5194/egusphere-2025-3637
Preprint. Discussion started: 21 August 2025

environmental management in China.

2 Experiments and methods

2.1 Station location

We set up an intensity Carbin installed muti particle instruments, move around three observation sites to collect data. They are distributed separately in three major Chinese cities, BJ, GZ, and SH. The scanning mobility particle sizer (SMPS) is used to measure the particle sizes of atmospheric aerosols. The micro pulse lidar (MPL) can be connected to computers to monitor PBLH data in real-time via specialized software. The equipment setup is shown in Fig. 1a and 1b.

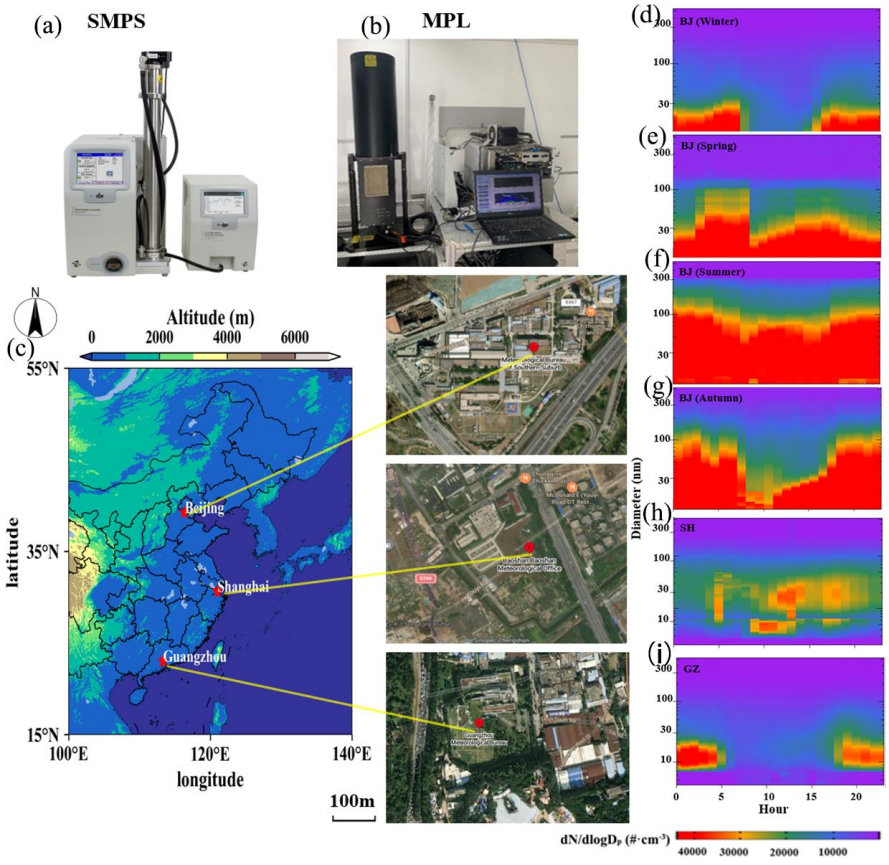

https://doi.org/10.5194/egusphere-2025-3637
Preprint. Discussion started: 21 August 2025

Fig. 1 The instrument: (a) SMPS and (b) MPL. (c) Depiction of instruments, geographical location diagram and surroundings of three observation sites in BJ, GZ and SH. (d-g) The diurnal variation of PNC during observations in BJ in different seasons from July 2017 to October 2019, (h) in SH from April to June 2020, and (i) in GZ from November 2019 to March 2020, respectively.

The observation site was established at Beijing Observatory (116.35° E, 39.2° N, 44 m a.s.l.), located along the Fifth Ring Road in the Daxing District's Old Palace area, the southern suburb of BJ, within the North China Plain. The terrain is elevated in the northwest and lower in the southeast, surrounded by mountains to the west, north, and northeast. The site experiences a temperate, semi-humid to semi-arid monsoon climate. The surrounding traffic network is intricate, with significant traffic congestion. The diurnal variation of PNSD in different seasons in BJ is significant (Fig. 1d–Fig. 1g). In winter (December, January, and February), From 8:00 to 15:00 local time (LT), the PNC of smaller than 30 nm particles remained below 1,000 cm^{-3}, which was one of the reasons why NPF was lower than in other seasons. In summer, the PNC of smaller than 50 nm particles stayed above 4,000 cm^{-3}. These UFPs are typically primary particles that facilitate the growth of new particles in the atmosphere.

The site in GZ is the observation field of Guangzhou Meteorological Bureau (113°E, 23°N, 11 m a.s.l), 10 km from the center of GZ. An urban trunk road lies 500 m north of the site and another 100 m west, with the Chimelong Tourist Area and several industrial parks in proximity. GZ is in the central part of Guangdong Province and the northern edge of the PRD, with terrain that slopes from northeast to southwest. GZ is one of China's earliest open coastal cities, serving as a critical hub for transport and logistics. The city enjoys a subtropical monsoon climate with significant maritime influences. The particles were mainly concentrated at night, while the air was much cleaner during daylight hours. Starting from 17:00 LT, particles in the 25-50 nm range began to increase, likely due to the influence of land-sea circulation, which recirculated 25-50 nm particles. This phenomenon will be explained about the PBLH in the

https://doi.org/10.5194/egusphere-2025-3637
Preprint. Discussion started: 21 August 2025

following sections.

The observation site of SH is set at Baoshan Meteorological Bureau Observatory (121° E, 30.6° N, 2 m a.s.l). SH is situated in the alluvial plain of the YRD in Eastern China, bordered by Asia to the west and the Pacific Ocean to the east, with a population exceeding 24 million. The city experiences a subtropical monsoon climate, characterized by ample sunlight and precipitation. Compared to PNSD in BJ and GZ, the air in SH was the cleanest, with consistently low average PNC throughout the day (shown in Fig. 1h). PNC in SH was primarily concentrated during daylight hours, differing from their distribution in GZ. The PNC for particles smaller than 30 nm increased mainly between 21:00 LT and 2:00 LT.

2.2 Equipment and Dataset

The Scanning Mobility Particle Sizer (SMPS) is used to measure the particle sizes of atmospheric aerosols. The Micro Pulse Lidar (MPL) can be connected to computers to monitor PBLH data in real-time via specialized software. The equipment setup is shown in Fig. 1a and 1b. The measurements of aerosol particle number size contribution (PNSD) were made with SMPS. It measures particle size contribution from 11.3 nm to 552.3 nm in 1 min intervals and a Nano-SMPS has been added from December 2, 2018, to obtain the 2-40 nm PNSD. The autonomous MPL operates at 532 nm in both parallel and perpendicular polarizations, providing backscattered radiation profiles at a temporal resolution of 10–30 s and a vertical resolution of 30 m (Roldán-Henao et al., 2024). PBLH was derived from MPL measurements, except for SH during 1–29 April 2020 due to the Lidar misfunction during these period, where it was retrieved from ERA5 reanalysis data.

The effective PNSD observation datasets used in the analysis include 408 days (July 2017–October 2019) in BJ, 127 days (November 2019–March 2020) in GZ, and 53 days (April 2020–May 2020) in SH, respectively. The observation datasets used to plot

https://doi.org/10.5194/egusphere-2025-3637
Preprint. Discussion started: 21 August 2025

the PNSD are three-dimensional, including datetime, particle size range (Dp, the particle diameter), and particle number concentration (in dN/dlogDp) for the corresponding particle size. After obtaining the original data, we need to eliminate the abnormal values. In this study, the hourly average of real-time data was used to construct the PNSD plot, The characteristics of aerosol PNSD can determine its CS, GR, P value and physical in the atmosphere. The sources of aerosol particles can be identified through the analysis of their size distribution.

2.3 Identify NPF events and calculation of NPF parameters

In general, specific criteria are applied to identify NPF events. A typical NPF event should exhibit the following three characteristics, often summarized as a "banana" shape (Maso et al., 2005). First, there is an increase in nucleation-mode PNC (particles with 10–25 nm diameter). Second, new nucleation-mode particles develop independently and persist for several hours. Finally, nucleation particles show a continuously increasing trend over 3 hours (Maso et al., 2005). If a process meets the above criteria, it is classified as an NPF event, and that day is defined as an NPF day. If there was no clear growth of newly formed particles or the particle growth is intermittent in time, the day was classified as undefined. Days without a burst of nucleation-mode particles and subsequent growth were considered non-event days (Non_NPF).

Calculated GR during NPF using the geometric mean diameters of the fitted particle size distributions:

$$GR_{\Delta D_p} = \frac{dD_p}{dt} = \frac{dD_P}{\Delta t}$$

where D_p is the measured diameter during NPF at time t. We represent GR by calculating the linear fitting slope of the geometric mean diameter of particles within a

https://doi.org/10.5194/egusphere-2025-3637
Preprint. Discussion started: 21 August 2025

certain time period (Casquero-Vera et al., 2023).

CS represents the loss of gaseous vapors due to their condensation onto aerosol particles. It is positively correlated with the collision sink and does not directly affect PNC. The formula is as follows (Kulmala et al., 2012):

$$CS = 4\pi D \int_{0}^{d_p max}{}_{m} d_p N_{d_p} dd_p = 4\pi D \sum_{d_p} \beta_{m,d_p} d_p N_{d_p}$$

Where D is the diffusion coefficient of the condensed gas, β_m is the correction coefficient.

2.4 Survival Parameter

Survival parameter is crucial for determining the occurrence of NPF events, as it represents the fraction of newly formed particles that survive the transition from a smaller to a larger diameter. (Tuovinen et al., 2022). It can be used to predict the dimensionless P of pollutant gas and provide guidance during periods of particulate pollution (Kulmala et al., 2017). The formula of the dimensionless P is as follows:

$$\mathrm{P} = \frac{\mathrm{CS'}}{\mathrm{GR'}}$$

Where the $CS' = CS/(10^{-4} s^{-1})$, and $GR' = GR/(1\,nm\,h^{-1})$. Both CS and GR are key parameters calculated from PNSD. Generally, high CS values tend to suppress NPF, but the survival probability can vary significantly due to environmental conditions and particle interactions (Tuovinen et al., 2022). It is significant for investigating the pollution source to research the P, as well as the impact of meteorological conditions and seasonal changes of P value.

2.5 Backward trajectories

https://doi.org/10.5194/egusphere-2025-3637
Preprint. Discussion started: 21 August 2025

This study used global reanalysis of meteorological data to calculate the pollutant source and air mass transport trajectories at three sites. We used a method combining the Potential Source Contribution Function (PSCF) and Concentration-Weighted Trajectory (CWT) in the HYSPLIT model to identify pollutant sources reaching observation sites and assess their impact on NPF. PSCF shows the contribution from potential source areas based on the conditional probability of pollution trajectories in each grid but does not indicate the pollution level in the study area. The ij_{th} component of a PSCF field given as follows (Zong et al., 2018):

$$PSCF_{ij} = m_{ij} / n_{ij}$$

where n_{ij} is the total number of endpoints that fall in the ij_{th} cell, and m_{ij} is the number of endpoints in that plot for which the readings exceed a user defined threshold standard. Note that cells with few endpoints can result in high uncertainty in the PSCF method. Thus, to move these high uncertainties, an arbitrary weight function $W(n_{ij})$ is multiplied into the PSCF value:

$$W_{ij} = \begin{cases} 1.0, & N_{ij} > 3N_{Ave} \\ 0.70, & 1.5N_{Ave} < N_{ij} < 3N_{Ave} \\ 0.42, & N_{Ave} < N_{ij} < 1.5N_{Ave} \\ 0.17, & 0 < N_{ij} < N_{Ave} \end{cases}$$

3 Result and discussion

3.1 Frequency of NPF events

As discussed in Sect. 2, NPF events were identified using the methodology and criteria outlined by (Kulmala et al., 2012). The frequency of NPF events and average PBLH at the three measurement sites are illustrated in Fig. 2. During the observation period, all NPF events occurred during the daytime growth. The average PBLH was calculated

https://doi.org/10.5194/egusphere-2025-3637
Preprint. Discussion started: 21 August 2025

from 8:00 to 18:00 LT, which also could be the NPF window 9:00-15:00 LT.

We have found 74 NPF events during 408 effective observation days in BJ, from July 2017 to October 2019 (details in Table 1 which lists all NPF days during the observation period in BJ, GZ, and SH). The NPF frequency in BJ was 17.8%, with 12 events occurring in summer (June, July, and August). The summer months had the lowest occurrence, indicating that factors such as meteorological conditions and precursor availability, alongside PBLH, potentially influence NPF events (Deng, 2020) . NPF events occurred predominantly in spring and autumn months, with the notably highest frequencies observed in March (25.9%) and October (23.3%). Temperature emerged as the primary factor driving seasonal variations in the frequency and intensity of NPF in BJ (Li et al., 2023a). The monthly mean PBLH for Beijing averaged around 643 m, peaking at approximately 833 m and displaying a positive correlation with the NPF frequencies. For certain months, especially November and December, the substantial number of missing observations restricts the ability to comprehensively assess the influence of the boundary layer on NPF events. A more detailed discussion will be provided in the following sections.

A total of 14 NPF events were recorded during 127 effective observation days in GZ from November 2019 to March 2020. The mean NPF frequency was relatively low, averaging around 10.0%, with frequencies ranging from 3.4% to 20.0%. The mean PBLH was approximately 512 m, peaking at approximately 586 m, reinforcing the link between atmospheric mixing conditions and particle formation processes.

A total of 10 NPF events, with a frequency of 18.87%, were observed in SH over 53 days from April to June 2020. The mean PBLH in SH was approximately 677 m, reaching a maximum near 741 m at noon, with the highest values coinciding notably with high NPF frequencies, particularly in April.

https://doi.org/10.5194/egusphere-2025-3637
Preprint. Discussion started: 21 August 2025

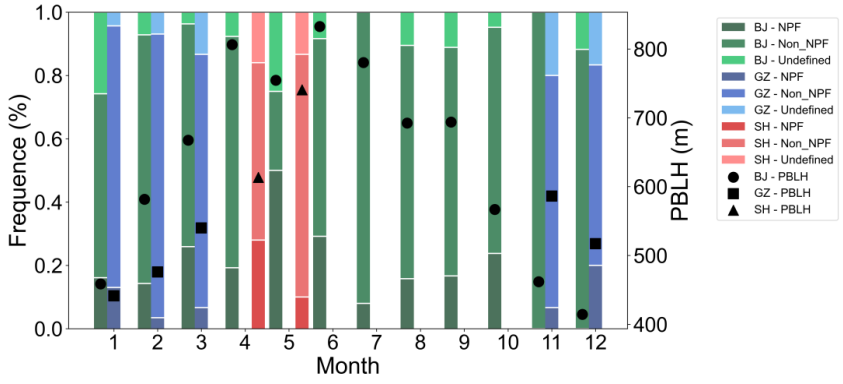

Fig. 2. Frequency of NPF events and average PBLH in BJ, GZ, and SH. The circle denotes PBLH of BJ, the square denotes PBLH of GZ, and the triangle denotes PBLH of SH.

Table 1. New particle formation events at BJ, GZ and SH.

site	Month	PBLH (m)	NPF days	Non_NPF days	Undefined days	Missing days
BJ	Jan	458.6719	5	18	8	0
BJ	Feb	581.5099	4	22	2	0
BJ	Mar	667.5479	7	19	1	4
BJ	Apr (in 2 years)	806.1902	5	19	2	35
BJ	May	754.4776	2	1	1	26
BJ	Jun (in 2 years)	832.5667	7	15	2	30
BJ	Jul (in 2 years)	780.34	7	30	0	32
BJ	Aug (in 2 years)	692.309	5	14	2	31
BJ	Sep	693.769	3	13	2	13
BJ	Oct	566.9179	5	15	1	10
BJ	Nov (in 2 years)	461.7263	0	2	0	58
BJ	Dec (in 2 years)	414.4698	0	15	2	45
GZ	Jan	441.4076	3	19	1	8
GZ	Feb	476.0462	1	26	2	0
GZ	Mar	539.949	2	24	4	1
GZ	Nov	586.0955	2	22	6	0

https://doi.org/10.5194/egusphere-2025-3637
Preprint. Discussion started: 21 August 2025

GZ	Sep	517.0407	6	19	5	1
SH	Apr	613.2995	7	15	4	5
SH	May	740.7455	3	23	4	1

3.2 PBLH under different events

The relationship between PBLH and NPF is further explored with a temporal resolution approach. The observation period was classified into NPF days and Non_NPF days, and Fig. 3 reveals clear distinctions in the diurnal variations of PBLH between NPF and Non_NPF days. Prior to sunrise (0:00-6:00 LT), PBLH remained at 150–200 m. With the onset of surface heating after 6:00 LT, the PBLH grown rapidly, especially on NPF days, reaching roughly 500 m by 9:00 LT compared to approximately 390 m on Non_NPF days. After 9:00 LT, the solar radiation that the surface receives increases, making PBLH rise gradually (Zheng et al., 2017). On NPF days, the maximum average PBLH in BJ was 1165 m, whereas on Non_NPF days, it peaked at approximately 962 m around 14:00 LT, marking a difference of about 203 m. In the late afternoon (16:00–18:00 LT), the PBLH values declined as insolation wanes. In GZ, the boundary layer remained relatively elevated on Non_NPF days, often exceeding 600 m even during nighttime. Vehicular emissions outside the observation sites contribute to an “aerosol greenhouse effect”, enhancing nighttime thermal retention (Miao et al., 2019). Meanwhile, the urban heat island effect intensifies surface thermal turbulence, promoting the nocturnal rise of the boundary layer (Huang and Bai, 2023; Zhang et al., 2024). Across all three sites, the PBLH on NPF days was 100–200 m higher than on Non-NPF days. This difference was consistently observed across BJ, GZ, and SH, suggesting that enhanced convective mixing and reduced particle CS under high PBLH conditions provide favorable conditions for nucleation and particle growth.

https://doi.org/10.5194/egusphere-2025-3637
Preprint. Discussion started: 21 August 2025

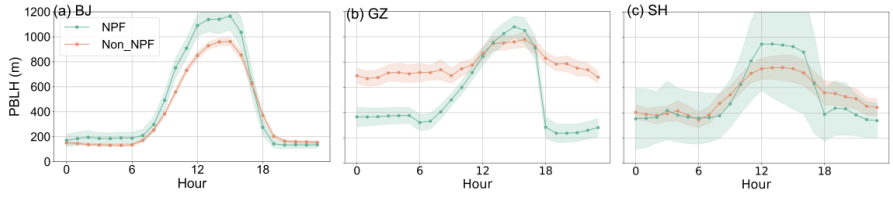

Fig. 3. The average of PBLH during NPF events and Non_NPF events at (a) BJ, (b) GZ, and (c) SH.

3.3 Evolution Patterns and Particle Growth

Within the dataset comprising 71 NPF events, four instances were observed to occur concurrently with the boundary layer's ascent, classified as Type I. A second pattern, designated as Type II, involves NPF events manifesting as atmospheric turbulence intensifies, coinciding with boundary layer elevations exceeding 800 m Fig. 4a illustrates a representative case of Type I on 24 August 2017, where at approximately 10:30 LT, the PBLH commenced its ascent from 450 meters. Concurrently, the particle number concentration of nucleation mode particles (Nuc mode) surged from 294,644 cm^{-3} to 503,055 cm^{-3}, indicating the initiation of an NPF event synchronized with the development of the boundary layer. Conversely, a Type II event was characterized by a rapid increase in Nuc at 11:30 LT, accompanied by the emergence of a distinct new particle mode, indicative of the onset of NPF at this time. The PBLH increased from 22 m at 7:00 LT to approximately 1,000 m by 11:30 LT. Fig. 4c and 4d depict the temporal correlation between average PBLH and Vehicular emissions outside the observation sites contribute to an “aerosol greenhouse effect,” enhancing nighttime thermal retention. Meanwhile, the urban heat island effect intensifies surface thermal turbulence, promoting the nocturnal rise of the boundary layer. for the respective event types. The t represents the relative time at which the NPF event occurs, and t+1 refers to one hour after the onset of the NPF event. Comparative analysis reveals that Type I events predominantly occur when the PBLH is around 400 m, suggesting that initial boundary layer development can serve as a catalyst for NPF. In contrast, Type II events are initiated when the PBLH exceeds 800 m, implying a requirement for a more mature

https://doi.org/10.5194/egusphere-2025-3637
Preprint. Discussion started: 21 August 2025

boundary layer to facilitate nucleation processes. The gradual increase in PBLH leads to a significant reduction in near-surface aerosol concentrations and facilitates the accumulation of precursor vapors within a larger volume, thereby decreasing condensation loss and creating favorable conditions for Nuc (Hao et al., 2018; Rose et al., 2021; Zhang et al., 2024). As the PBLH approaches its maximum, photochemical reactions become most intense, resulting in peak concentrations of oxidized precursor gases (Rose et al., 2021). This fulfills the critical conditions for nucleation and subsequently triggers NPF events. Meanwhile, the concentration of low-volatility oxygenated organic aerosol is positively correlated with PBLH (Lin et al., 2021), suggesting that in Type II events, NPF may be primarily driven by low-volatility organics or H_2SO_4.

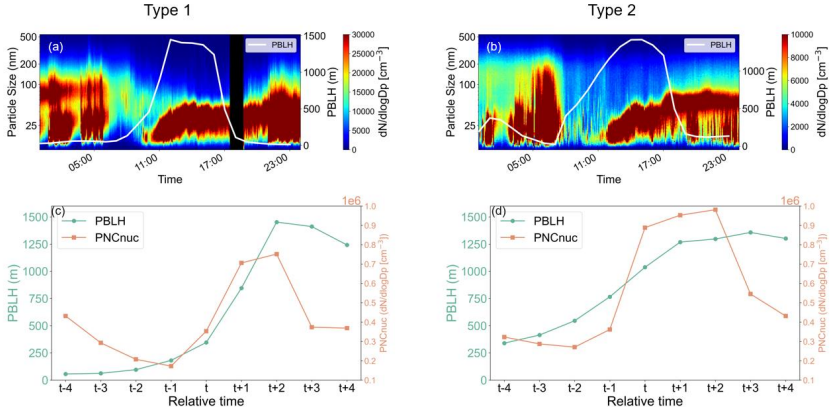

Fig. 4. Time series of aerosol particle number size distribution: (a) a case from Type I on 24 August 2017 and (b) a case from Type2 on 27 April 2018. Time series of averaged PBLH and Nuc mode for (c) Type1 and (d) type2. The t denotes the relative time at which NPF occurs.

3.4 Particle number size distribution of new particles formation events

Fig. 5 presents a classification of NPF event types based on particle size distribution evolution across three cities categorized as Type I, Type II, and Shrinkage events as

https://doi.org/10.5194/egusphere-2025-3637
Preprint. Discussion started: 21 August 2025

Type III. During the observation period, two inverse growth events were documented in BJ, whereas only one such event was recorded in both GZ and SH. At the BJ, GZ, and SH sites, Type I events typically started approximately two hours earlier than Type II events. At BJ, nighttime bursts of polluted particles were observed on all 4 days; however, the end times of these events could not be quantitatively determined. In contrast, at both GZ and SH, the end times of Type I and Type II events were nearly identical, coinciding with the rapid drop of the boundary layer to its minimum height. The remaining two events, which occurred in BJ, involved particle growth from approximately 100 nm at 17:00 LT to less than 25 nm during nighttime. In GZ, particles formatted at 9:00 LT, reaching sizes up to 100 nm, followed by a reduction to below 30 nm after 15:00 LT. In SH, particle growth commenced at 10:00 LT, increasing from 10 nm to approximately 50 nm, before shrinking and reverting to nucleation mode by 15:00 LT. This investigation primarily examines the influence of PBLH on NPF events, deliberately excluding the analysis of inverse growth mechanisms. Consequently, these events are omitted from further detailed examination.

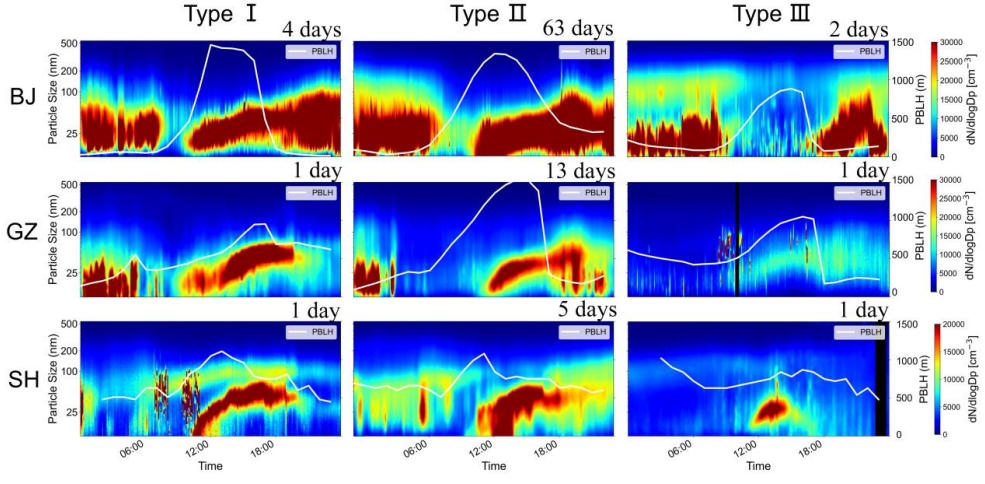

Fig. 5. Averaged aerosol particle number size distribution. PNSD of two types of NPF and growth, and shrinkage days in BJ, GZ, and SH, respectively. Averaged PBLH add in the white line.

https://doi.org/10.5194/egusphere-2025-3637
Preprint. Discussion started: 21 August 2025

3.5 The correlation between PBLH and P

The relationship between PBLH and P during NPF events is illustrated in Fig. 6. In three cities, there was a negative correlation has been firstly built between PBLH and P parameters. The PBLH of BJ had the highest average with a value of 1010 m, and the P was highly variable, with a maximum of 153.92 and a minimum of 8.80. The P for BJ and GZ were similar. SH recorded the lowest average PBLH, with an average of 721.92 m. Among the three cities, SH was the cleanest, with P = 23.96. The higher influence of urban vehicular emissions in BJ and GZ may explain this difference. In contrast, SH's proximity to the sea led to higher relative humidity, which promoted NPF but also accelerated particle dissipation. However, the correlations in BJ and GZ were weak, with R^2 values of 0.21 and 0.024, respectively. In SH, the shorter observation period limited the number of captured events, showing a strong negative correlation in the available data, with an R^2 value of 0.99. As the PBLH increased, the P exhibited varying decreasing trends across the three cities. A high PBLH leads to a low P, which favors the occurrence of NPF events. The differences in correlation at different locations can be explained by site-specific factors. For instance, the GZ site is located near a major traffic artery, where particulate pollution from traffic sources weakens the correlation between P and PBLH. The decrease in the boundary layer provides a more stable environment for the particle accumulation, leading to a higher P value without suppose the NPF.

https://doi.org/10.5194/egusphere-2025-3637
Preprint. Discussion started: 21 August 2025

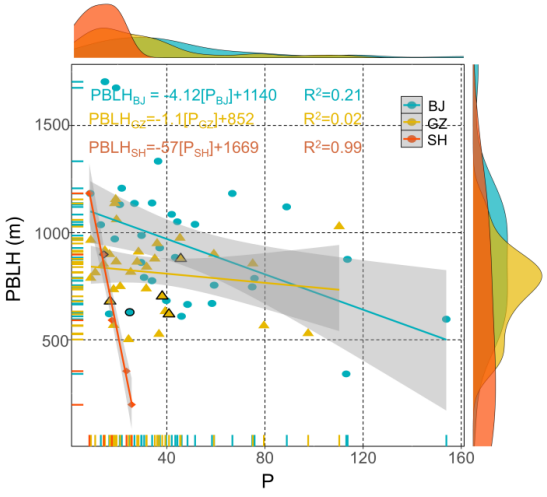

Fig. 6 The correlation analysis between PBLH and P in (a) BJ, (b) GZ, and (c) SH. The circle denotes BJ, the triangle denotes GZ, and the diamond denotes SH. The dots with black borders represent Type I.

3.6 The backward trajectories of particles during NPF events

Nucleation-mode aerosols mainly originate from early nucleation and the subsequent growth of NPF events. To track this, we meagered nucleation-mode concentration data to 48-hour back trajectories during NPF periods. Overall, nucleation-mode particle contributions to total concentration were greater in the northern parts of the study sites compared to the southern parts. Fig. 8 presents the PSCF and frequency distribution of NPF events across three cities.

Fig. 7a shows the PSCF results for the BJ site, indicating significant contributions from Mongolia and cities within Anhui Province. In particular, pollution sources within Mongolia and along the Mongolia-Russia border showed probabilities greater than 0.4. The nucleation-mode particles were mainly from the northwest and the north of the observation station. The pollutant source impacting BJ had the fastest transmission speed within 48 hours and the broadest geographic reach, with primary contributions

https://doi.org/10.5194/egusphere-2025-3637
Preprint. Discussion started: 21 August 2025

originating from Russia and passing through Mongolia to BJ's northwest. Fig. 7b highlighted BJ and Zhangjiakou as the cities with the highest NPF event contribution among surrounding locations, where favorable geographic and environmental conditions promote the formation of particles smaller than 100 nm. The north-northwest of BJ exhibited the highest frequency of NPF events, exceeding 25%, while the area with the second-highest frequency extended approximately 420 km from the observation station, measured by latitude.

In GZ, as shown in Fig. 7c and 7d, pollutant contributions were primarily from Jiangxi and Fujian provinces to the northeast, with additional high-contribution areas extending eastward into Hubei Province. The distribution of atmospheric particle pollutants in this area is highly concentrated. The region with a high frequency (> 25%) of NPF events lies within 100 km to the northeast of the observation site, corresponding to the eastern portion of Guangdong Province.

For SH, pollutant contributions are mainly from the west-northwest, similar to BJ, although the overall pollutant contribution is lower than that for BJ. The contribution area spans Jiangsu Province and extends into southern Hebei Province. Additionally, there are notable contributions from the southwest, passing through Anhui and Jiangxi Provinces. Around SH, NPF event contribution levels are relatively high (approximately 10-25%), with the northern region showing the highest frequency, exceeding 25%. 10%-25% of the contribution came from the sea, indicating that marine circulation is one of the important pathways for the transport of new particles.

https://doi.org/10.5194/egusphere-2025-3637
Preprint. Discussion started: 21 August 2025

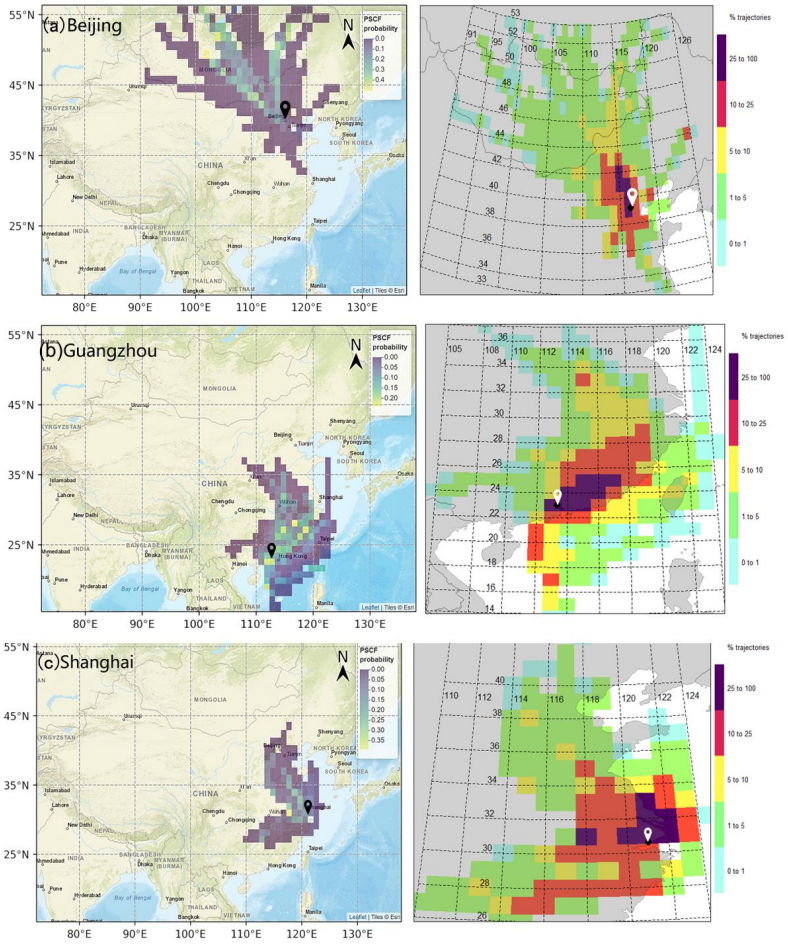

409

410 **Fig. 7** The 48h backward trajectory by using PSCF, and the map of NPF event contribution levels
411 when particle size is below 100nm in BJ, GZ, and SH during NPF days.

412 **4 Conclusions**

413 This study examined the relationship between PBLH and NPF events key parameters
414 in Chinese's megacities (BJ, GZ, and SH, respectively). During the observation period,
415 March and May in BJ exhibited the highest frequencies of NPF occurrence, accounting
416 for 25.9% and 23.8%, respectively. Diurnal analyses confirmed that NPF days were

https://doi.org/10.5194/egusphere-2025-3637
Preprint. Discussion started: 21 August 2025

consistently associated with significantly higher midday PBLH compared to Non_NPF days. Across all three sites, the average PBLH on NPF days was 150–200 m higher than on Non-NPF days, highlighting the importance of convective mixing and aerosol dilution in promoting nucleation. We also identified two distinct mechanisms: We identified two distinct mechanisms of NPF initiation: Type I and Type II. Type I refers to events triggered during the initial rise of the boundary layer, where turbulent mixing associated with PBLH development facilitates nucleation. Type II involves nucleation that occurs only after the boundary layer reaches a certain height (>800 m). Correlation analyses emphasized the boundary layer was a key factor in triggering NPF the level especially at SH 0.99 This was particularly evident at SH, where the PBLH shows a strong negative correlation with the P value. Indicating the vertical mixing process and the development of the boundary layer has a dominant impact on the key parameter of NPF events.

We obtained the 48h backward trajectories of particles at three sites during NPF by using the HYSPLIT model. The main source of pollutant contribution in BJ is Mongolia in the northwest direction. GZ's contribution source is distributed in Jiangxi and Fujian Provinces in the northeast of the site, and SH's is in the northwest. The average frequency level of NPF is over 25%, which is in the north of each site, indicating that the overall level of air pollution in the north is higher than that in the south. Our finding provides a brand-new insight into atmospheric turbulence and boundary layer development could has dominate influence on the NPF and UFP formation mechanism, which should not be ignored in further research.

Data availability

The measured data described in this manuscript can be accessed at the data repository maintained by Mendeley Data. Doi: 10.17632/zpwjj5ymmp.1 (Hu, 2025)

CRediT authorship contribution statement

https://doi.org/10.5194/egusphere-2025-3637
Preprint. Discussion started: 21 August 2025

HH collected the resources, wrote, and finalized this paper. HH, YZ, TL, and DP analyzed the data and generated the figures. HW planned the study, provided instruments and data, and discussed the results. HH plotted the figures. HH, HW conducted the measurements. HW revised this paper.

Declaration of competing interest

The authors declare that they have no known competing financial interests or personal relationships that could have appeared to influence the work reported in this paper.

Acknowledgments

This research was supported by the National Natural Science Foundation of China (42105073), Protect of the Sichuan Department of Science and Technology (2022NSFSC1074). It was also supported by the Key Laboratory of China Meteorological Administration Atmospheric Sounding.

References:

Blanco-Alegre, C., Calvo, A. I., Alonso-Blanco, E., Castro, A., Oduber, F., and Fraile, R.: Evolution of size-segregated aerosol concentration in NW Spain: A two-step classification to identify new particle formation events, J Environ Manage, 304, 114232, 10.1016/j.jenvman.2021.114232, 2022.

Bousiotis, D., Dall'Osto, M., Beddows, D. C. S., Pope, F. D., and Harrison, R. M.: Analysis of New Particle Formation (NPF) Events at Nearby Rural, Urban Background and Urban Roadside Sites, Atmospheric Chemistry and Physics, 10.5194/acp-2018-1057, 2018.

Casquero-Vera, J. A., Pérez-Ramírez, D., Lyamani, H., Rejano, F., Casans, A., Titos, G., Olmo, F. J., Dada, L., Hakala, S., Hussein, T., Lehtipalo, K., Paasonen, P., Hyvärinen, A., Pérez, N., Querol, X., Rodríguez, S., Kalivitis, N., González, Y., Alghamdi, M. A., Kerminen, V.-M., Alastuey, A., Petäjä, T., and Alados-Arboledas, L.: Impact of desert dust on new particle formation events and cloud condensation nuclei budget in dust-influenced areas, EGUsphere, 10.5194/egusphere-2023-1238, 2023.

Chan, T., Cai, R., Ahonen, L. R., Liu, Y., Zhou, Y., Vanhanen, J., Dada, L., Chao, Y., Liu, Y., Wang, L., Kulmala, M., and Kangasluoma, J.: Assessment of particle size magnifier inversion methods to obtain the particle size distribution from atmospheric measurements, Atmospheric Measurement Techniques, 13, 4885-4898, 10.5194/amt-13-4885-2020, 2020.

Chu, B., Kerminen, V.-M., Bianchi, F., Yan, C., Petäjä, T., and Kulmala, M.: Atmospheric new particle

https://doi.org/10.5194/egusphere-2025-3637
Preprint. Discussion started: 21 August 2025

formation in China, Atmospheric Chemistry and Physics, 19, 115-138, 10.5194/acp-19-115-2019, 2019.

Chu, B., Chen, T., Liu, Y., Ma, Q., Mu, Y., Wang, Y., Ma, J., Zhang, P., Liu, J., Liu, C., Gui, H., Hu, R., Hu, B., Wang, X., Wang, Y., Liu, J., Xie, P., Chen, J., Liu, Q., Jiang, J., Li, J., He, K., Liu, W., Jiang, G., Hao, J., and He, H.: Application of smog chambers in atmospheric process studies, Natl Sci Rev, 9, nwab103, 10.1093/nsr/nwab103, 2022.

Deng: Seasonal Characteristics of New Particle Formation and Growth in Urban Beijing, ENVIRONMENTAL SCIENCE & TECHNOLOGY, 54, 2020.

Deng, C., Cai, R., Yan, C., Zheng, J., and Jiang, J.: Formation and growth of sub-3 nm particles in megacities: impact of background aerosols, Faraday Discuss, 0, 364-381, 10.1039/d0fd00083c, 2021a.

Deng, C., Cai, R., Yan, C., Zheng, J., and Jiang, J.: Formation and growth of sub-3 nm particles in megacities: impact of background aerosols, Faraday Discuss, 226, 348-363, 10.1039/d0fd00083c, 2021b.

Deot, N., Kanawade, V. P., Papetta, A., Baalbaki, R., Pikridas, M., Marenco, F., Kulmala, M., Sciare, J., Lehtipalo, K., and Jokinen, T.: Effect of planetary boundary layer evolution on new particle formation events over Cyprus, Aerosol Research Discuss., 2024, 1-35, 10.5194/ar-2024-31, 2024.

Du, W., Zhao, J., Dada, L., Xu, W., Wang, Y., Shi, Y., Chen, X., Kokkonen, T. V., Cai, J., Zhang, Y., Wang, Q., Cai, R., Zha, Q., Zhou, L., Li, Z., Yu, F., Fu, P., Hu, F., Wang, Z., Worsnop, D. R., Bianchi, F., Kerminen, V.-M., Kulmala, M., and Sun, Y.: Impacts of enhanced new-particle growth events above urban roughness sublayer on cloud condensation nuclei, One Earth, 8, 10.1016/j.oneear.2024.12.005, 2025.

Hao, L., Garmash, O., Ehn, M., Miettinen, P., Massoli, P., Mikkonen, S., Jokinen, T., Roldin, P., Aalto, P., Yli-Juuti, T., Joutsensaari, J., Petäjä, T., Kulmala, M., Lehtinen, K. E. J., Worsnop, D. R., and Virtanen, A.: Combined effects of boundary layer dynamics and atmospheric chemistry on aerosol composition during new particle formation periods, Atmospheric Chemistry and Physics, 18, 17705-17716, 10.5194/acp-18-17705-2018, 2018.

Hu, H.: New insights into the boundary layer revolution correlation with new particle formation characteristics in megacities of China, Mendeley Data, V1, 10.17632/zpwjj5ymmp.1, 2025.

Hu, M., Shang, D., Guo, S., and Wu, Z.: Mechanism of New Particle Formation and Growth as well as Environmental Effects under Complex Air Pollution in China, Acta Chimica Sinica, 74, 10.6023/a16020105, 2016.

Huang, L. and Bai, L.: Evaluation of planetary boundary layer schemes on the urban heat islands in the urban agglomeration over the greater bay area in South China, Frontiers in Earth Science, 10, 10.3389/feart.2022.1065074, 2023.

https://doi.org/10.5194/egusphere-2025-3637
Preprint. Discussion started: 21 August 2025

Kanawade, V. P., Sebastian, M., Hooda, R. K., and Hyvärinen, A.-P.: Atmospheric new particle formation in India: Current understanding and knowledge gaps, Atmospheric Environment, 270, 10.1016/j.atmosenv.2021.118894, 2022.

Kerminen, V.-M., Chen, X., Vakkari, V., Petäjä, T., Kulmala, M., and Bianchi, F.: Atmospheric new particle formation and growth: review of field observations, Environmental Research Letters, 13, 10.1088/1748-9326/aadf3c, 2018.

Kulmala, M., Kerminen, V. M., Petaja, T., Ding, A. J., and Wang, L.: Atmospheric gas-to-particle conversion: why NPF events are observed in megacities?, Faraday Discuss, 200, 271-288, 10.1039/c6fd00257a, 2017.

Kulmala, M., Cai, R., Stolzenburg, D., Zhou, Y., Dada, L., Guo, Y., Yan, C., Petäjä, T., Jiang, J., and Kerminen, V.-M.: The contribution of new particle formation and subsequent growth to haze formation, Environmental Science: Atmospheres, 10.1039/d1ea00096a, 2022.

Kulmala, M., Petaja, T., Nieminen, T., Sipila, M., Manninen, H. E., Lehtipalo, K., Dal Maso, M., Aalto, P. P., Junninen, H., Paasonen, P., Riipinen, I., Lehtinen, K. E., Laaksonen, A., and Kerminen, V. M.: Measurement of the nucleation of atmospheric aerosol particles, Nat Protoc, 7, 1651-1667, 10.1038/nprot.2012.091, 2012.

Kulmala, M., Dada, L., Daellenbach, K. R., Yan, C., Stolzenburg, D., Kontkanen, J., Ezhova, E., Hakala, S., Tuovinen, S., Kokkonen, T. V., Kurppa, M., Cai, R., Zhou, Y., Yin, R., Baalbaki, R., Chan, T., Chu, B., Deng, C., Fu, Y., Ge, M., He, H., Heikkinen, L., Junninen, H., Liu, Y., Lu, Y., Nie, W., Rusanen, A., Vakkari, V., Wang, Y., Yang, G., Yao, L., Zheng, J., Kujansuu, J., Kangasluoma, J., Petaja, T., Paasonen, P., Jarvi, L., Worsnop, D., Ding, A., Liu, Y., Wang, L., Jiang, J., Bianchi, F., and Kerminen, V. M.: Is reducing new particle formation a plausible solution to mitigate particulate air pollution in Beijing and other Chinese megacities?, Faraday Discuss, 226, 334-347, 10.1039/d0fd00078g, 2021.

Li, C., Zhao, Y., Li, Z., Liu, L., Zhang, X., Zheng, J., Kerminen, V.-M., Kulmala, M., Jiang, J., Cai, R., and Xiao, H.: The dependence of new particle formation rates on the interaction between cluster growth, evaporation, and condensation sink, Environmental Science: Atmospheres, 3, 168-181, 10.1039/d2ea00066k, 2023a.

Li, C., Li, Y., Li, X., Cai, R., Fan, Y., Qiao, X., Yin, R., Yan, C., Guo, Y., Liu, Y., Zheng, J., Kerminen, V.-M., Kulmala, M., Xiao, H., and Jiang, J.: Comprehensive simulations of new particle formation events in Beijing with a cluster dynamics–multicomponent sectional model, Atmospheric Chemistry and Physics, 23, 6879-6896, 10.5194/acp-23-6879-2023, 2023b.

Lin, Z., Wang, Y., Zheng, F., Zhou, Y., Guo, Y., Feng, Z., Li, C., Zhang, Y., Hakala, S., Chan, T., Yan, C., Daellenbach, K. R., Chu, B., Dada, L., Kangasluoma, J., Yao, L., Fan, X., Du, W., Cai, J., Cai, R., Kokkonen, T. V., Zhou, P., Wang, L., Petäjä, T., Bianchi, F., Kerminen, V.-M., Liu, Y., and Kulmala, M.: Rapid mass growth and enhanced light extinction of atmospheric aerosols during the heating season haze

https://doi.org/10.5194/egusphere-2025-3637
Preprint. Discussion started: 21 August 2025

episodes in Beijing revealed by aerosol–chemistry–radiation–boundary layer interaction, Atmospheric Chemistry and Physics, 21, 12173-12187, 10.5194/acp-21-12173-2021, 2021.

Maso, M. D., Hussein, T., Kulmala, M., Aalto, P. P., Riipinen, I., Wagner, R., and Lehtinen, K. E. J.: Formation and growth of fresh atmospheric aerosols eight years of aerosol size distribution data from SMEAR II, Hyytiälä, Finland, BOREAL ENVIRONMENT RESEARCH, 10, 323-336, 10.1239/res.10:323–336, 2005.

Miao, Y., Li, J., Miao, S., Che, H., Wang, Y., Zhang, X., Zhu, R., and Liu, S.: Interaction Between Planetary Boundary Layer and PM2.5 Pollution in Megacities in China: a Review, Current Pollution Reports, 5, 261-271, 10.1007/s40726-019-00124-5, 2019.

Myhre, G., Samset, B. H., Schulz, M., Balkanski, Y., Bauer, S., Berntsen, T. K., Bian, H. M., 2013 #139}, Bellouin, N., Chin, M., Diehl, T., Easter, R. C., Feichter, J., Ghan, S. J., Hauglustaine, D., Iversen, T., Kinne, S., Kirkevåg, A., Lamarque, J. F., Lin, G., Liu, X., Lund, M. T., Luo, G., Ma, X., van Noije, T., Penner, J. E., Rasch, P. J., Ruiz, A., Seland, Ø., Skeie, R. B., Stier, P., Takemura, T., Tsigaridis, K., Wang, P., Wang, Z., Xu, L., Yu, H., Yu, F., Yoon, J. H., Zhang, K., Zhang, H., and Zhou, C.: Radiative forcing of the direct aerosol effect from AeroCom Phase II simulations, Atmospheric Chemistry and Physics, 13, 1853-1877, 10.5194/acp-13-1853-2013, 2013.

Peng, Y., Liu, X., Dai, J., Wang, Z., Dong, Z., Dong, Y., Chen, C., Li, X., Zhao, N., and Fan, C.: Aerosol size distribution and new particle formation events in the suburb of Xi'an, northwest China, Atmospheric Environment, 153, 194-205, 10.1016/j.atmosenv.2017.01.022, 2017.

Quan, J. and Jia, X.: Review of aircraft measurements over China: aerosol, atmospheric photochemistry, and cloud, Atmospheric Research, 243, 10.1016/j.atmosres.2020.104972, 2020.

Roldán-Henao, N., Su, T., and Li, Z.: Refining Planetary Boundary Layer Height Retrievals From Micropulse-Lidar at Multiple ARM Sites Around the World, Journal of Geophysical Research: Atmospheres, 129, 10.1029/2023jd040207, 2024.

Rose, C., Collaud Coen, M., Andrews, E., Lin, Y., Bossert, I., Lund Myhre, C., Tuch, T., Wiedensohler, A., Fiebig, M., Aalto, P., Alastuey, A., Alonso-Blanco, E., Andrade, M., Artíñano, B., Arsov, T., Baltensperger, U., Bastian, S., Bath, O., Beukes, J. P., Brem, B. T., Bukowiecki, N., Casquero-Vera, J. A., Conil, S., Eleftheriadis, K., Favez, O., Flentje, H., Gini, M. I., Gómez-Moreno, F. J., Gysel-Beer, M., Hallar, A. G., Kalapov, I., Kalivitis, N., Kasper-Giebl, A., Keywood, M., Kim, J. E., Kim, S.-W., Kristensson, A., Kulmala, M., Lihavainen, H., Lin, N.-H., Lyamani, H., Marinoni, A., Martins Dos Santos, S., Mayol-Bracero, O. L., Meinhardt, F., Merkel, M., Metzger, J.-M., Mihalopoulos, N., Ondracek, J., Pandolfi, M., Pérez, N., Petäjä, T., Petit, J.-E., Picard, D., Pichon, J.-M., Pont, V., Putaud, J.-P., Reisen, F., Sellegri, K., Sharma, S., Schauer, G., Sheridan, P., Sherman, J. P., Schwerin, A., Sohmer, R., Sorribas, M., Sun, J., Tulet, P., Vakkari, V., van Zyl, P. G., Velarde, F., Villani, P., Vratolis, S., Wagner, Z., Wang, S.-H., Weinhold, K., Weller, R., Yela, M., Zdimal, V., and Laj, P.: Seasonality of the particle number concentration and size distribution: a global analysis retrieved from the network of Global Atmosphere

https://doi.org/10.5194/egusphere-2025-3637
Preprint. Discussion started: 21 August 2025

574 Watch (GAW) near-surface observatories, Atmosphereic Chemistry and Physics, 22, 17185-17223,
575 10.5194/acp-2020-1311, 2021.

576 Sebastian, M., Kanawade, V. P., and Pierce, J. R.: Observation of sub-3nm particles and new particle
577 formation at an urban location in India, Atmospheric Environment, 256,
578 10.1016/j.atmosenv.2021.118460, 2021.

579 Shen, X., Sun, J., Zhang, X., Kiveka¨s, N., Zhang, Y., Wang, T., Zhang, X., Yang, Y., Wang, D., Zhao, Y.,
580 and Qin, D.: Particle Climatology in Central East China Retrieved from Measurements in Planetary
581 Boundary Layer and in Free Troposphere at a 1500-m-High Mountaintop Site, Aerosol and Air Quality
582 Research, 16, 689-701, 10.4209/aaqr.2015.02.0070, 2016.

583 Shengjie, N., Chengchang, Z., Jiming, S., 牛生杰, 章澄昌, and 孙继明: Observational Researches on
584 the Size Distribution of Sand Aerosol Particles in the Helan Mountain Area, 大气科学学报, 25, 243-252,
585 2001.

586 Stjern, C. W., Hodnebrog, O., Myhre, G., and Pisso, I.: The turbulent future brings a breath of fresh air,
587 Nat Commun, 14, 3735, 10.1038/s41467-023-39298-4, 2023.

588 Sun, Y., Du, W., Wang, Q., Zhang, Q., Chen, C., Chen, Y., Chen, Z., Fu, P., Wang, Z., Gao, Z., and
589 Worsnop, D. R.: Real-Time Characterization of Aerosol Particle Composition above the Urban Canopy
590 in Beijing: Insights into the Interactions between the Atmospheric Boundary Layer and Aerosol
591 Chemistry, Environ Sci Technol, 49, 11340-11347, 10.1021/acs.est.5b02373, 2015.

592 Tuovinen, S., Cai, R., Kerminen, V.-M., Jiang, J., Yan, C., Kulmala, M., and Kontkanen, J.: Survival
593 probabilities of atmospheric particles: comparison based on theory, cluster population simulations, and
594 observations in Beijing, Atmospheric Chemistry and Physics, 22, 15071-15091, 10.5194/acp-22-15071-
595 2022, 2022.

596 Wang, Y., Wang, J., Li, Z., Jin, X., Sun, Y., Cribb, M., Ren, R., Lv, M., Wang, Q., Gao, Y., Hu, R., Shang,
597 Y., and Gong, W.: Contrasting aerosol growth potential in the northern and central-southern regions of
598 the North China Plain: Implications for combating regional pollution, Atmospheric Environment, 267,
599 10.1016/j.atmosenv.2021.118723, 2021.

600 Wu, H., Li, Z., Jiang, M., Liang, C., Zhang, D., Wu, T., Wang, Y., and Cribb, M.: Contributions of traffic
601 emissions and new particle formation to the ultrafine particle size distribution in the megacity of Beijing,
602 Atmospheric Environment, 262, 10.1016/j.atmosenv.2021.118652, 2021a.

603 Wu, H., Li, Z., Li, H., Luo, K., Wang, Y., Yan, P., Hu, F., Zhang, F., Sun, Y., Shang, D., Liang, C., Zhang,
604 D., Wei, J., Wu, T., Jin, X., Fan, X., Cribb, M., Fischer, M. L., Kulmala, M., and Petaja, T.: The impact
605 of the atmospheric turbulence-development tendency on new particle formation: a common finding on
606 three continents, Natl Sci Rev, 8, nwaa157, 10.1093/nsr/nwaa157, 2021b.

https://doi.org/10.5194/egusphere-2025-3637
Preprint. Discussion started: 21 August 2025

607 Zhang, H., Huang, W., Shen, X., Ramisetty, R., Song, J., Kiseleva, O., Holst, C. C., Khan, B., Leisner,
608 T., and Saathoff, H.: Aerosol composition, air quality, and boundary layer dynamics in the urban
609 background of Stuttgart in winter, Atmospheric Chemistry and Physics, 24, 10617-10637, 10.5194/acp-
610 24-10617-2024, 2024.

611 Zhao, G., Zhao, C., Kuang, Y., Tao, J., Tan, W., Bian, Y., Li, J., and Li, C.: Impact of aerosol hygroscopic
612 growth on retrieving aerosol extinction coefficient profiles from elastic-backscatter lidar signals,
613 Atmosphere Chemistry and Physics, 10.5194/acp-2017-240, 2017.

614 Zheng, C., Zhao, C., Zhu, Y., Wang, Y., Shi, X., Wu, X., Chen, T., Wu, F., and Qiu, Y.: Analysis of
615 influential factors for the relationship between PM2.5 and AOD in Beijing, Atmos. Chem. Phys., 17,
616 13473-13489, 10.5194/acp-17-13473-2017, 2017.

617 Zong, Z., Wang, X., Tian, C., Chen, Y., Fu, S., Qu, L., Ji, L., Li, J., and Zhang, G.: PMF and PSCF based
618 source apportionment of PM2.5 at a regional background site in North China, Atmospheric Research,
619 203, 207-215, 10.1016/j.atmosres.2017.12.013, 2018.

620

621